Silver-phosphate glass matrix for iodine conditioning: From sorbent design to vitrification

R. Pénélope, L. Campayo, M. Fournier, A. Gossard, A. Grandjean

Silver-phosphate glass matrix for iodine conditioning: from sorbent design to vitrification

R. Pénélope[1], L. Campayo[1], M. Fournier[1], A. Gossard[2], A. Grandjean[2]

[1] CEA, DES, ISEC, DE2D, University of Montpellier, Marcoule, Bagnols sur Cèze, France

[2] CEA, DES, ISEC, DMRC, University of Montpellier, Marcoule, Bagnols sur Cèze, France

raphael.penelope@cea.fr

CEA Marcoule, ISEC/DE2D/SEVT, Bât. 208, BP17171, 30207 Bagnols-sur-Cèze Cedex, France

Abstract

A new route for the synthesis of silver-phosphate based sorbent beads as precursors of final iodine waste form is proposed here. This sorbent is used to entrap gaseous iodine produced during the reprocessing of spent nuclear fuels and to be directly transformed into materials composed of a silver phosphate glass phase considered as high efficient iodine containment matrix for long-term storage in deep geological repository. Using sacrificial organic template method (alginate) and well controlled calcination of the obtained silver phosphate grains materials, this innovative synthesis makes in-situ formation of metallic silver inside them. Ag^0 then can easily entrap iodine when in contact with gaseous iodine. The obtained sorbent were tested for iodine trapping in static conditions. They showed great performances with a catch rate of 480 $mg.g^{-1}$. The iodine-loaded sorbent were finally heat treated at 650 °C with an iodine loss lower than 3 $\%_{wt}$. The resulted materials shows the presence of the expected silver phosphate glass matrix with a great iodine incorporation of 9 $\%_{mol}$.

Keywords: adsorption, disposal, environment, filter, immobilization, nuclear, matrix

1 Introduction

As global energy consumption is constantly increasing to face population growth [1], [2] there is a need to produce more electricity [3]. To fulfill this demand, nuclear energy can contribute to overcome this issue [4]. Fission-based nuclear energy production relies on fuels composed of uranium and plutonium oxide. After several years of use in plants, those fuels have to be stored [5], [6] or reprocessed to retrieve recoverable materials [7], [8], depending on local policies specific to each country. In the second case, the reprocessing also generates ultimate wastes composed of minor actinides and fission products that need to be safely managed. Among fission products generated during the dissolution in acidic conditions of spent fuels, there is gaseous iodine primarily present under two isotope forms. ^{129}I is an intermediate level waste with a half-life of 15.7×10^7 years and an activity of 6.7×10^7 $Bg.g^{-1}$. On the other hand, there is ^{131}I, a high-level waste with a half-life of 8.02 days and an activity of 4.6×10^{15} $Bg.g^{-1}$. Past nuclear accidents like that of Fukushima Daiichi power plant have well demonstrated the potential consequences of an exposition to those radionuclides for human beings [9]–[11]. Furthermore, because of iodine mobility in the environment [12]–[14] and the very long half-life of ^{129}I, it is important to have specific management of those radionuclides in the frame of the reprocessing of spent nuclear fuels.

Nowadays, two main management solutions are used. On one hand, in the United Kingdom or France, radioactive iodine management mainly relies on an isotopic dilution by discharge into the sea [15], [16]. This is performed in the frame of regulated release rights. However, for environmental and ethical issues, this can be seen as controversial by public opinions. Moreover, such a kind of management is quite impossible for inland reprocessing plants, not speaking of countries that rule out this option. On the other hand, the trapping of the gaseous radioactive iodine with solid sorbents can be considered. Literature counts many sorbents with

various chemical compositions as Metal-Organic Framework (MOF) [17], [18], silver-zeolite [19]–[21], chalcogenide aerogels (also called chalcogels) [22], [23], aerogels and xerogels [24]–[26], activated carbon [27]–[29], graphene [30]–[32], silver-silica and alumina [33]–[35] and many others. Several reviews highlight the different sorbents developed these last years [36]–[38]. Presently, iodine-loaded sorbents used in reprocessing plants are stored on site pending a definitive management stream.

In this latter case, the storage of an iodine-containing sorbents into a geological repository could be of interest. However, due to high specific surface areas favorable to iodine capture but detrimental to confinement properties, these sorbents have to be "monolithized" in a suitable form, i.e. as a conditioning matrix. Many works were devoted to the study of conditioning matrices [39]–[42] but the links with the upstream step of iodine capture is not always obvious. Here, we consider the case of silver-phosphate glasses for which, low melting temperatures make possible the incorporation of iodine into an amorphous phase [43]–[46]. This work presents the development of a silver-phosphate sorbent for gaseous iodine trapping made from an organic sacrificial template, with the aim of directly using this sorbent as a precursor for further vitrification, minimizing the number of handling steps once loaded with iodine ("from cradle to grave"). The efficiency of iodine trapping was determined in static conditions at 110 °C. Once loaded with iodine, the thermal transformation of such sorbent into a glassy conditioning matrix was also carried out. Physical properties of sorbent before and after iodine capture as well as the obtained matrix will be presented.

2 Materials and methods

2.1 *Synthesis of the sorbent*

The sorbent was made by an organic sacrificial template method derived from the one presented by Kimling et al. [47], [48] using sodium alginate as a precursor. Alginic acid sodium salt

(Sigma Aldrich), ethanol (96 % vol, VWR), calcium nitrate tetrahydrate (≥ 98 %, VWR) and silver phosphate, Ag_3PO_4 (≥ 99 %, Alfa Aesar) were used as reactants for the synthesis. A peristaltic pump REGLO Analog MS-4/8 from Ismatec® (Germany) with pipe of internal diameter of 2.79 mm from Cole-Parmer® (USA) allowed solution transfer from one tank to another.

A first suspension (Solution 1) was prepared by introducing silver phosphate with 250 mL of deionized water at a concentration of 6 $\%_{wt}$ and alginic acid sodium salt at 2 $\%_{wt}$. The addition of alginic acid sodium salt was done gradually to avoid the formation of aggregates and ensure a good homogeneity. The blend was stirred for 4 h at room temperature. Meanwhile, another 250 mL aqueous solution (Solution 2) containing calcium nitrate tetrahydrate with a concentration of 0.27 $mol.L^{-1}$ was prepared and stirred for 4 hours at room temperature. After stirring, Solution 1 was transferred by dripping into Solution 2 thanks to the peristaltic pump. This allows a cationic exchange between sodium and calcium [49], causing the cross-linking of alginate network [50], [51] and therefore, the retention of the bead shape. Then, the formed beads were retrieved by filtration and rinsed in a water bath under stirring for 1 h twice. A last washing under ethanol was finally performed and the beads were then placed in an oven at 60 °C during 16 h after vacuum filtration to eliminate solvent residues. The dry beads were then heat-treated at 500 °C for 90 min under air (heating rate of 5 $°C.min^{-1}$) to eliminate organics compounds. The principle of the synthesis is summarized in Fig. 1.

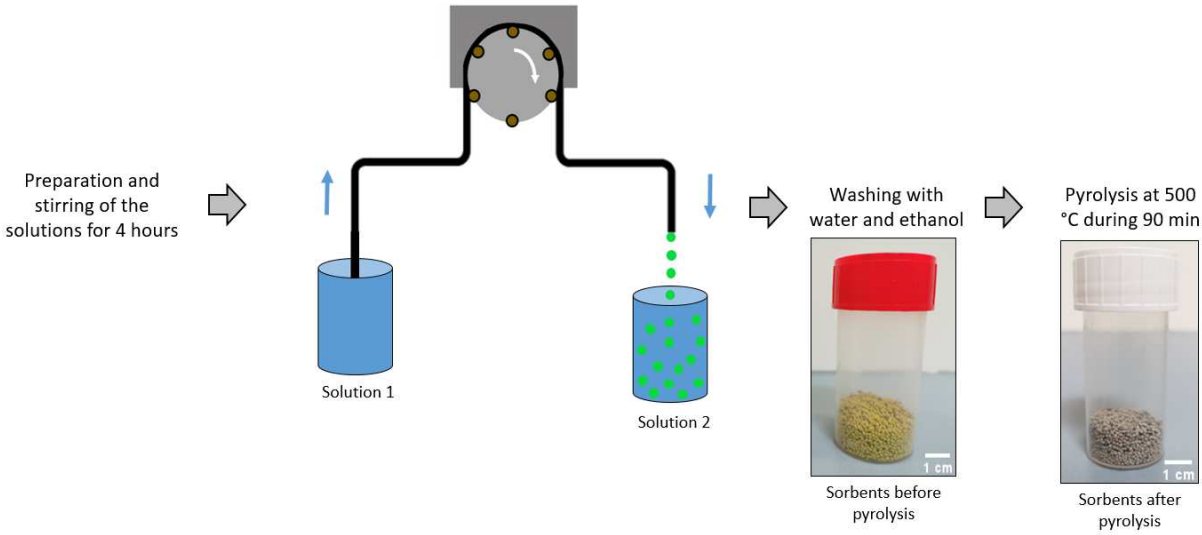

Fig. 1. Principle of the synthesis.

2.2 *Iodine capture static test*

Static iodine capture experiments were performed into a hermetic perfluoroalkoxy vial purchased from Savillex^{TM} (USA) with I_2 solid beads from Acros Chimica. The test was carried out by introducing 4.5 g of iodine beads at the bottom of the vial and 2.0 g of sorbents on a watch glass placed above without contact with iodine beads. The vial was hermetically closed and placed into an oven for 16 h at 110 °C. After this duration time, the vial was removed and cooled to room temperature for 1 h. Then, the vial was opened, the watch glass was removed and let under a ventilated fume cupboard for 2 h to remove any solid iodine residues that could have condensed at the surface of the sorbent upon cooling. The weight difference of the sorbent before and after the test allowed the determination of captured iodine. The experimental process is summarized in Fig. 2.

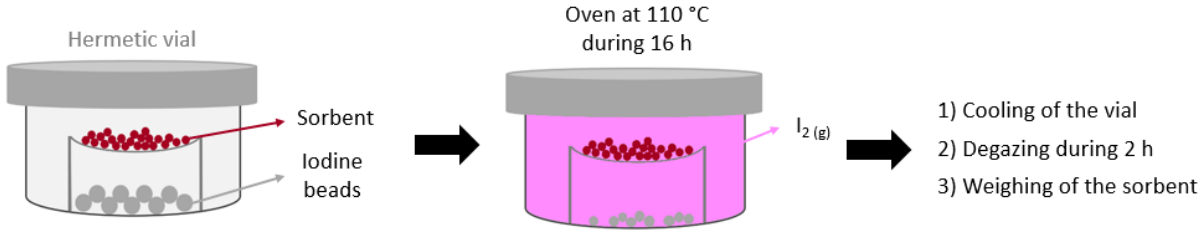

Fig. 2. Principle of the iodine capture test.

2.3 *Transformation of iodine-loaded sorbent*

After the iodine capture test described in section 2.2, iodine-loaded sorbent were placed in a platinum/rhodium crucible and heated up to 650 °C with a heating rate of 2 °C.min^{-1}. A dwell of 3 h was applied and the crucible was then removed from the furnace and cooled down at room temperature.

2.4 *Characterizations*

Specific surface area measurements were carried out with an ASAP Model 2010 device from Micromeritics® (USA). Before measurements, the sorbent were degassed for 24 h under 200 °C. Krypton was used as a probe during the analysis and Brunauer, Emmett and Teller (BET) theory was used to determine specific surface area ($0.05 < P/P_0 < 0.2$).

X-ray diffraction measurements (XRD) were acquired using crushed samples with a X'Pert PRO MPD PANalytical instrument in Bragg-Brentano geometry with a copper anode tube (Cu-Kα radiation at 0.154 nm) operating at 40 kV and 40 mA. Samples were crushed into powder with mortar before the experiments. Data were collected for a 2Θ range of 10-90° at ambient temperature. The obtained diffractograms were analyzed with the DIFFRAC.EVA V4.2 software (Bruker^{TM}, USA) by matching crystalline phases with The International Centre for Diffraction Data (ICDD) database PD4+ 2020.

The microstructure of the samples was examined by field emission gun-scanning electron microscopy (FEG-SEM) using a Zeiss Supra 55 at 15 kV with a 8.8 mm working distance (probe current ~ 1 nA). To probe the inner part of the sorbent and allow precise mapping and quantification, samples were embedded in an epoxy resin and polished before coating with a 10 nm carbon layer. The determination of the chemical composition of the different phases within samples was deduced from energy dispersive X-ray spectroscopy (EDS) analyses on plane polished samples with a Bruker AXS X-FlashDetector 4010 system. Elemental quantification was obtained from real standards spectra acquired in the same conditions using

conventional PhiRhoZ correction. Results are given with an uncertainty of 2 % atomic. Data collection and treatment were done with the ESPRIT2.0 software (Bruker™, USA).

The thermal behavior of iodine-loaded sorbent was analyzed by differential thermal analysis (DTA) and thermogravimetric analysis (TGA) with a SETSYS Evolution apparatus from SETARAM™ (France). Around 70 mg of sorbents were placed inside a 100 µL platinum crucible. The experiment was carried under air atmosphere (30 $mL.min^{-1}$) in a temperature range of 20-650 °C with a heating rate of 5 $°C.min^{-1}$. Thermograms were analyzed with the SETSYS-1750Cs Evol.-TG-DTA software (SETARAM™, France).

3 Results

3.1 Synthesized sorbent

The spherical-shaped obtained sorbent were cohesive and presented a diameter of roughly 2 mm (Fig. 1), which can be seen as a good correlation with the inner diameter of the pipe used for the transfer of solution. MEB pictures of back-scattered electrons (BSE) images (Fig. 3) highlight the presence of three different contrasts that is significant of a heterogeneous chemical composition. Those contrasts are present on the surface as well as inside the sorbent. EDS analyses (Fig. 4), associated to XRD measurements (Fig. S1), indicate the presence of three crystalline phases: metallic silver (ICDD card 04-001-2617), $Ag_4P_2O_7$ (ICDD card 00-011-0637) and $CaAg(PO_3)_3$ (ICDD card 00-023-0126).

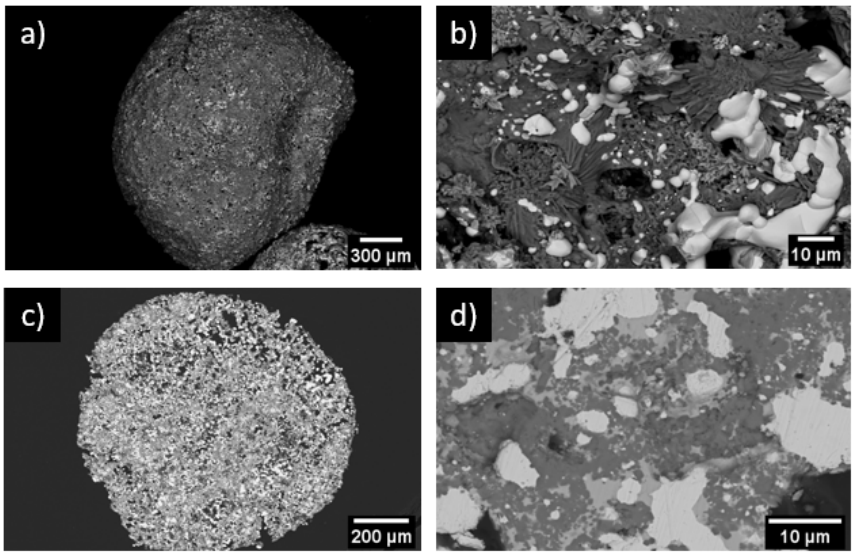

150

151 **Fig. 3.** SEM pictures of sorbent surface (a, b) and cross-sections (c, d) (BSE mode).

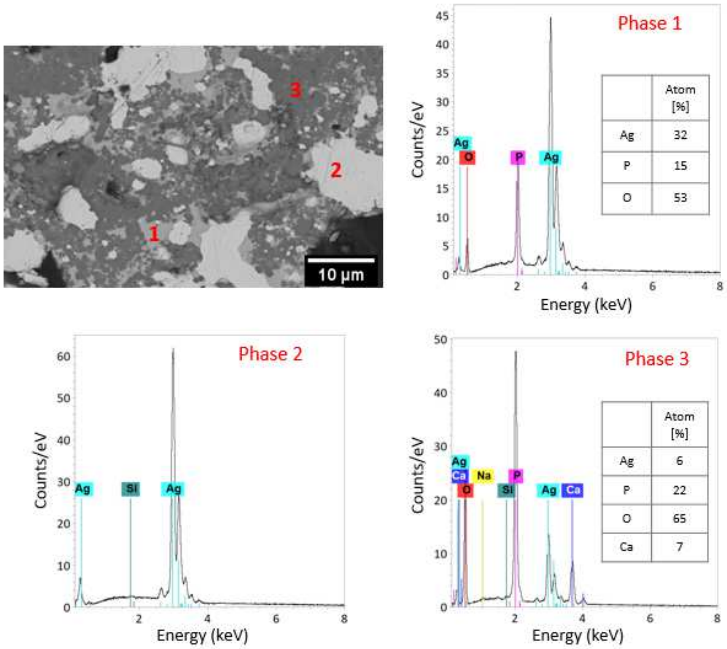

152

153 **Fig. 4.** EDS and quantification (inlet) results of sorbent as plane polished samples.

154 The initial precursor Ag_3PO_4 was not present anymore after pyrolysis meanwhile it was the
155 only mineral phase before (Fig. S2). Therefore, this implies that a chemical reaction occurred
156 during this heat treatment. Moreover, the presence of metallic silver involves a reductive
157 environment. Actually, this heat treatment had a double effect with the removal of organic
158 compounds (highlighted by a mass loss of the beads of 26 % after pyrolysis) and the in-situ
159 formation of silver metal (through silver reduction) in the sorbent. This can be seen as in-situ

functionalization (i.e., the formation of a chemical function dedicated to iodine capture) resulting from the fact that Ag^0 is indeed known to easily entrap iodine by the formation of AgI when in contact with gaseous iodine [52], [53].

EDS results also reveals the presence of Na and Si residues. Sodium comes from the alginic acid sodium salt used as a reagent and reveals that not all the sodium was substituted by calcium during the cross-linking of the alginate network. Silicon is a contamination brought during the synthesis.

In addition to the previously described phases assemblage, SEM images indicate a low porosity level inside the sorbent. This observation was confirmed by BET(Kr) measurement which resulted in a specific surface area of 0.14 $m^2.g^{-1}$.

3.2 Iodine capture test in static conditions

Gravimetric tests for I_2 capture in static conditions aimed at determining the I_2 uptake of the developed sorbent. After 16 h at 110 °C, the sorbent showed a mass gain of 47 % that is to say a capture rate of 470 mg of iodine per gram of sorbent assuming that iodine was the only element to be fixed. This experiment was carried out twice and was found reproducible (capture rate of 480 $mg.g^{-1}$ for the second test). SEM pictures of the sorbent after I_2 capture (Fig. 5) show "swollen" surfaces with homogeneous chemical contrast.

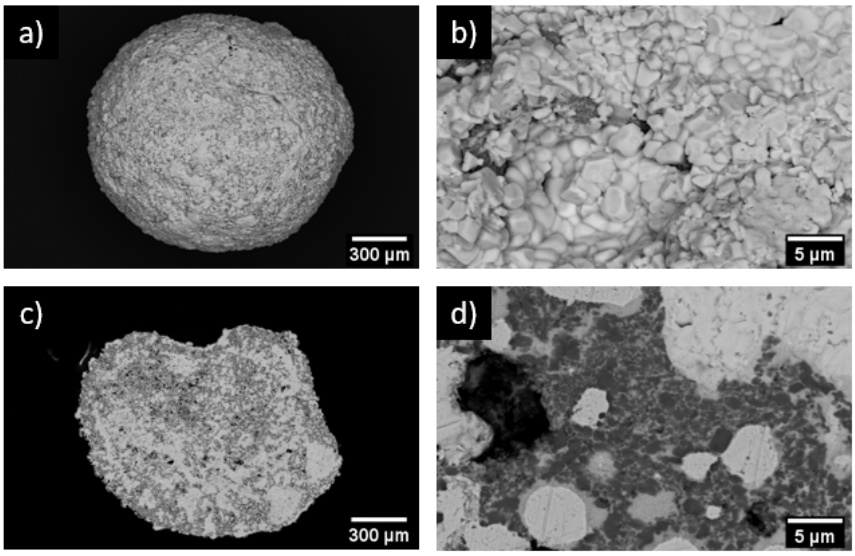

Fig. 5. SEM pictures of sorbent surface (a, b) and cross-section (c, d) after I_2 capture (BSE mode).

The surface is composed of a unique phase combining silver and iodine (Fig. S3). Cross-section analyses indicate the presence of different phases evidenced by several chemical contrasts. To precisely determine the distribution of the different elements, X-Ray mapping analyses were carried out (Fig. 6).

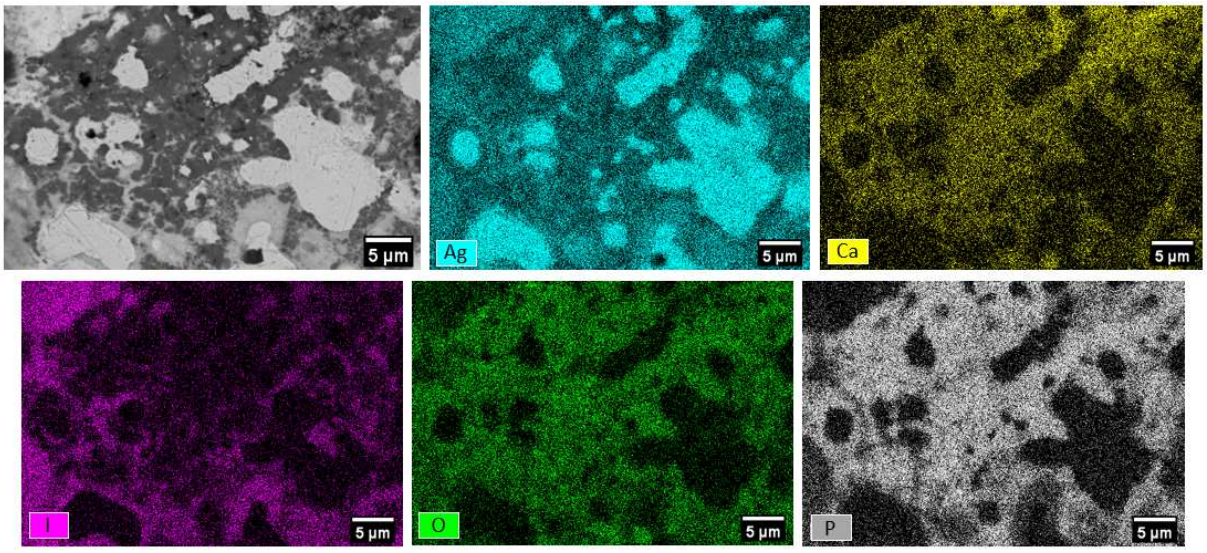

Fig. 6. X-Ray elemental mapping analysis of cross-sections of the sorbent after I_2 capture.

Among the most contrasted areas from SEM pictures (i.e. brightest), some are only composed of silver whereas others contain silver and iodine. This highlights that not all Ag^0 has reacted with iodine in spite of a large excess of iodine during the test (see paragraph 3.3). This might be explained by a lack of accessibility of all Ag^0 particles to $I_2(g)$. The X-Ray map analysis of the darkest area indicates the presence of silver, calcium, oxygen and phosphorus. From XRD analysis (Fig. 7), this latter phase has been identified as $CaAg(PO_3)_3$ (ICDD card 00-023-0126). XRD diffractogram also shows the presence of silver iodide (ICDD card 00-009-0399 and 04-005-4493) which confirms thermodynamic considerations that forecast its formation from Ag^0 and gaseous iodine [52], [53]. Therefore, the phase with a bright contrast associating silver and iodine has been attributed to silver iodide.

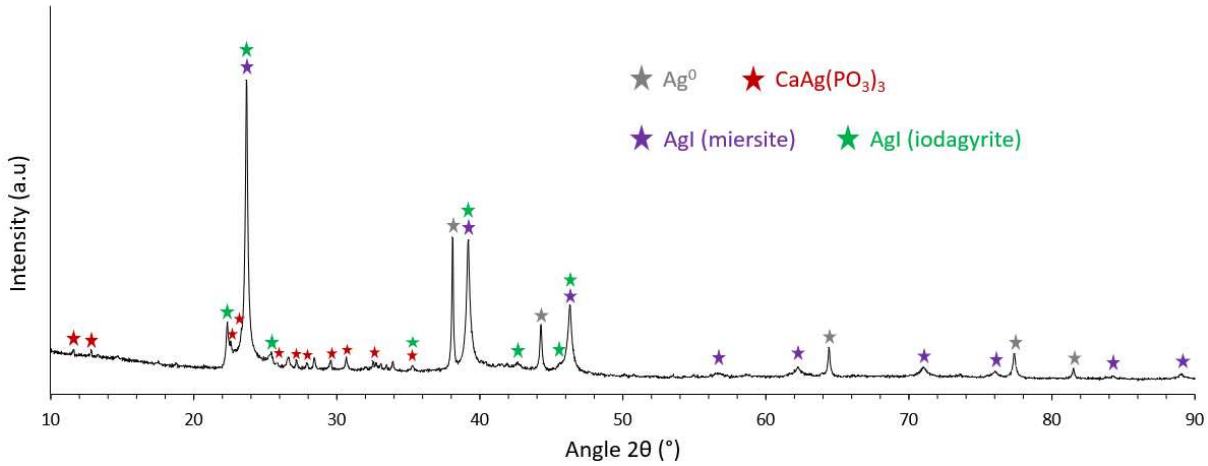

Fig. 7. XRD analysis of sorbent after iodine capture.

It is worth noting that a fourth phase is present on SEM images and seems preferentially localized around Ag^0 particles. It contains silver, iodine, oxygen and phosphorus. Nonetheless, such a kind of phase is not visible on the XRD diffractogram. This could be explained by a small proportion of this phase compared to the others or a low crystallinity.

3.3 Reactive silver content

To precisely determine the proportion of Ag^0 that has reacted with I_2, complementary gravimetric tests of I_2 capture were performed. For this, the sorbent were finely ground with a mixer mill (30 Hz during 2 min) to be converted into powder. In so doing, it was expected that all the Ag^0 particles could be in contact with I_2(g). Also, the same experimental conditions were used for the I_2 capture test as before. A weight increase of around 52 % was measured which corresponds to a capture rate of 520 $mg.g^{-1}$. XRD results (Fig. S4) confirmed that no more Ag^0 was visible (i.e. the content in Ag^0 was under detection limit of roughly 1 wt.%) and that the operating conditions for the I_2 capture test correspond to a large excess of iodine compared to the silver species content (calculated from initial Ag_3PO_4 used). Hence, from this value, it is possible to calculate that the sorbent were composed of around 48 $\%_{wt}$ of Ag^0. Moreover, the fraction of metallic silver that reacted with I_2(g) in the bead-shape sorbent can be assessed and is equal to 85 %.

3.4 *Transformation of iodine-loaded sorbent into a conditioning matrix*

Preliminary TDA/TGA tests were done to assess the behavior of iodine-loaded sorbent during a thermal treatment. The obtained results are presented in Fig. 8 and indicate a weight loss lower than 0.2 %.

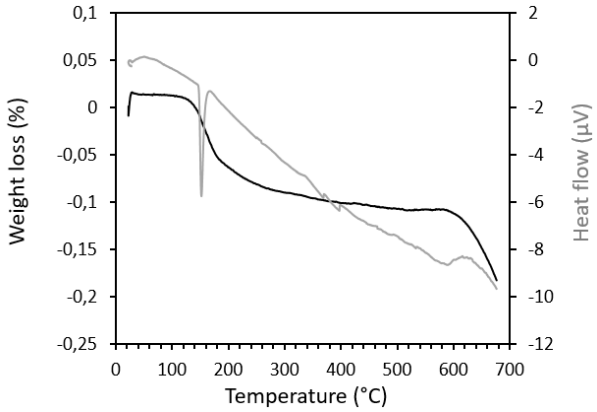

Fig. 8. TDA/TGA results of iodine-loaded sorbent.

A first slope change of the TGA curve can be observed at around 150 °C. At this temperature, a thin endothermic pic is also present on the TDA curve. It is attributed to the allotropic transformation of AgI from β to α and γ polytypes at 147 °C [54]. The small weight loss observed between 20 and 150 °C is assumed to be due to the degassing of poorly sorbed species (H_2O, CO_2 …) at the surface of the sorbent.

A second slope change of the TGA curve is observed from 600 °C and is accompanied by a large endothermic pic on the TDA curve. This pic highlights the beginning of iodine release. Thus, for the vitrification step, it has been decided to set the maximum temperature at 650 °C. This choice was made to ensure a good vitrification of the sorbent and to avoid too significant iodine losses (< 0.2 $\%_{wt}$ according TGA results).

In agreement with these results, a thermal treatment at 650 °C was performed on iodine-loaded sorbent to transform them into a conditioning matrix belonging to the AgI-Ag_2O-P_2O_5 glassy system. A weight loss lower than 3 $\%_{wt}$ was measured at the end of the test and no trace of a purple deposit or yellow/orange dots (potentially corresponding to iodine) was visible on the

walls of the furnace and the crucible. After air-cooling, the obtained matrix (Fig. S5.) showed a molten surface with spherical asperities that could be seen as the remainders of the initial sorbent. SEM and EDS analyses of a cross-section of the obtained matrix are shown in Fig. 9.

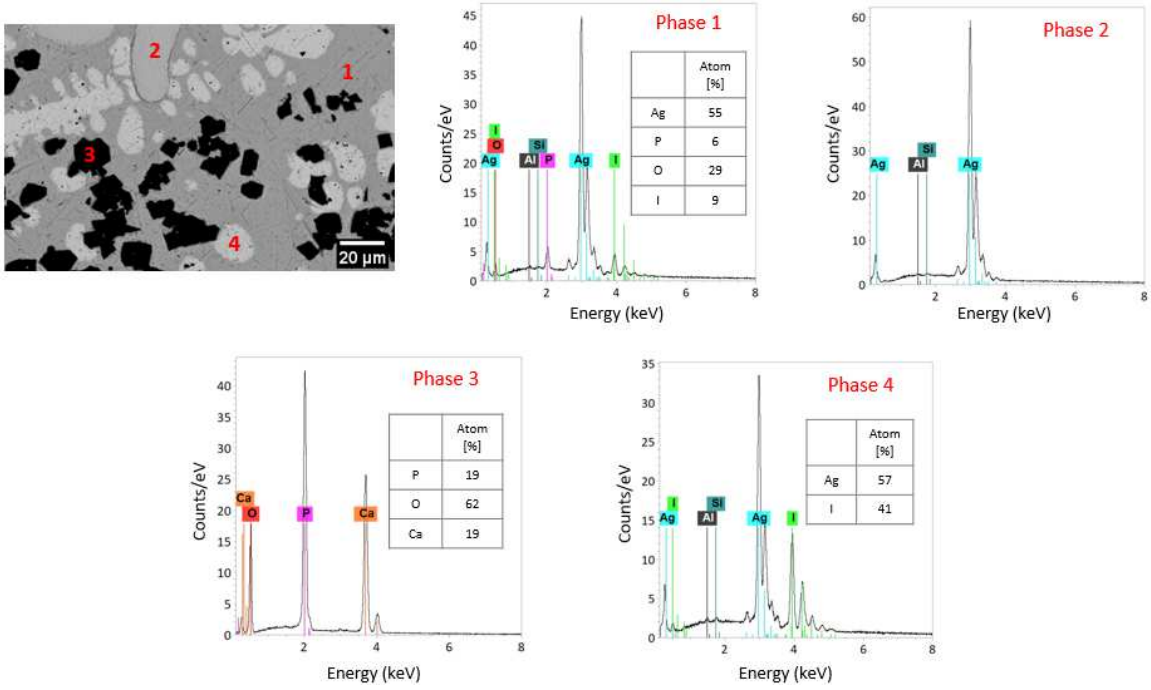

Fig. 9. EDS and quantification (inlet) results of the obtained matrix.

From the contrasts on SEM image (BSE mode), it is possible to bring out four different phases. Phase 1 in Fig. 9, composed of silver, iodine, phosphorus and oxygen has a composition that can be written as $Ag_{9.2}I_{1.5}PO_{4.8}$ (normalization for one phosphorus atom). For their own, combining their elemental composition and XRD results (Fig. 10), it was possible to conclude that phases 2, 3 and 4 correspond to metallic silver (00-004-0783), $Ca_2P_2O_7$ (04-009-3876) and AgI (00-009-0399 and 04-007-2546) respectively. The quantification of phase 4 indicates that there is more silver than what would be theoretically expected (50 %). This probably means that there is an excess of unreacted metallic silver that is intimately mixed with silver iodide (the size of these silver nodules and/or their weak contrast difference with silver iodide being responsible for the selection of a multiphasic analysis area in the present case). EDS quantification results are thus in good agreement with XRD analysis (Fig. 10) except for phase 1 that is not indexed. However, a broad halo pattern can be observed between 20° and 55° which

is the sign of the presence of an amorphous fraction. Therefore, phase 1 was ascribed to this amorphous phase that actually corresponds to a silver phosphate glass. This glass can incorporate an iodine content of 9 $\%_{mol}$ (15 $\%_{wt}$). Nonetheless, not all the iodine was incorporated into the glass matrix as demonstrated by AgI residues in phase 4 identified by SEM or XRD.

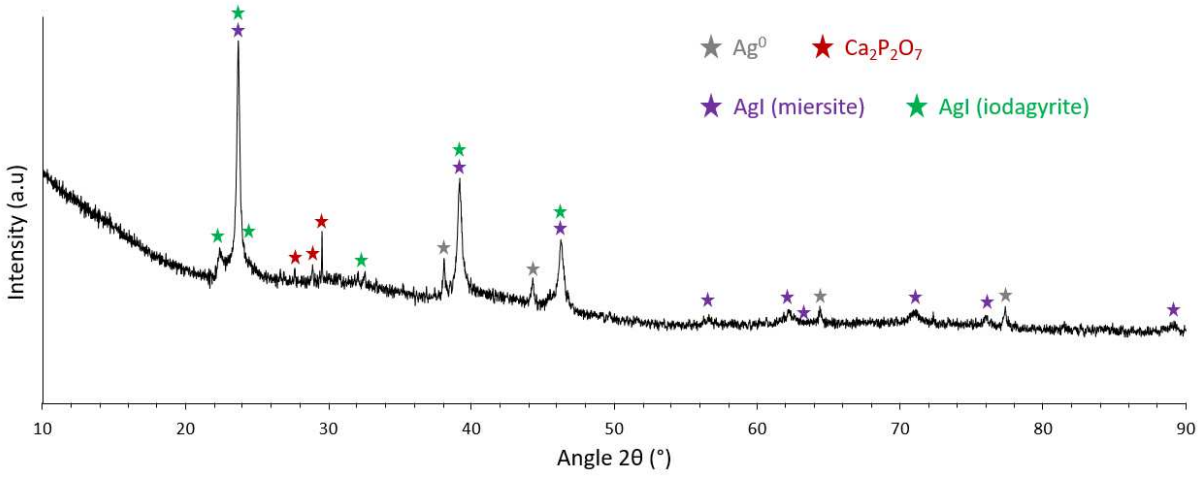

Fig. 10. XRD analysis of the matrix obtained after thermal treatment.

4 Discussion

4.1 Key roles of sodium alginate

During the first step, a peristaltic pump was used to transfer the silver phosphate/sodium alginate mixture into the calcium nitrate solution. When the drops fell into the solution, they kept the pseudo-spherical shape they had at the outlet of the tubing. This phenomenon is due to a cationic exchange between sodium and calcium [49]. It results in a cross-linking of the alginate network and leads to the formation of a hydrogel [50], [51]. Therefore, sodium alginate firstly plays the role of shaping reagent that stabilizes the bead structure by formation of a 3D network.

Secondly, the characterization of the obtained sorbents, after the pyrolysis step, showed the presence of metallic silver. However, in the previous steps, no metallic silver was introduced in the system. This highlights that silver reduction occurred during pyrolysis. This reaction is made possible by the presence of alginate molecules that also plays the role of a reducing agent. Such a role has already been emphasized in studies to produce metallic silver for medical uses. As a matter of fact, because of the antibacterial properties of silver nanoparticles [55], [56], many researches have been done to synthesize them. To do that, reducing agents have been widely used. Among them, sodium alginate is one of the most described [57]–[59]. This organic compound constituted of many hydroxyl and carboxylate groups (stabilized by sodium ions) is directly involved in the silver reduction process. This two-step reaction includes a first electrostatic interaction between Ag^+ and oxygen-containing groups by forming complexes [57], [58]. Then, hydroxyl groups are oxidized into carbonyl groups and silver is reduced.

The use of sodium alginate as a reducing agent requires an activation energy to initiate the reaction. It can be brought by different methods like Joule heating, microwave heating or UV-activation [57]–[59]. In our work, this activation was brought by Joule heating during the pyrolysis step (500°C).

4.2 Iodine reactivity

EDS and XRD analyses of the pristine sorbent indicate the presence of a $Ag_4P_2O_7$ phase whereas, after iodine capture, this phase was not present anymore. Meanwhile, a new iodine-silver phosphate was formed simultaneously to AgI and seemed principally localized around Ag^0 particles. The formation of this iodine-silver phosphate phase indicates that at least two chemical reactions occurred during the iodine capture test. This phase was highlighted with SEM analysis of cross sections (Fig. 4 and Fig. 5) but its chemical composition could not be obtained due to the small size of corresponding areas compared to the probed volume. Furthermore, no characteristic peak of a crystalline phase with such a qualitative composition

was present on the X-Ray diffractogram (Fig. 6). However, various studies have considered the AgI-$Ag_4P_2O_7$ binary system [60]–[62]. They indicate that it is possible to form several crystalline phases along this system ($Ag_{19}I_{15}P_2O_7$, $Ag_6I_2P_2O_7$ …) depending on the proportions of AgI and $Ag_4P_2O_7$ and the temperature. For our operating conditions, it is assumed that the content of AgI is much superior to that of $Ag_4P_2O_7$. In that case, and for a temperature of 110 °C, the $Ag_{19}I_{15}P_2O_7$ phase might have been formed. Such an assumption is reinforced by the fact that the AgI-$Ag_4P_2O_7$ binary diagram shows a domain where this phase should coexist with AgI crystals as it was observed for our sorbent. The reason why this phase was not visible on the X-Ray diffractogram might then merely rely on a too weak proportion.

4.3 Vitrification

The obtained matrix presents various phases including an iodine-containing silver phosphate glass, AgI and Ag^0. From the AgI-Ag_2O-P_2O_5 ternary diagrams [45], [46], it seems possible to obtain a homogeneous glass for a specific composition range by varying the O/P ratio or the AgI content. Even if these ternary diagrams are only available at 350 and 500 °C, they both present wide homogeneous vitrification areas. Consequently, we assumed here that this behavior could be extrapolated to close temperature ranges (but the boundaries of the homogeneous vitrification area could be slightly different). Hence, for our matrix made at 650 °C, it should be possible to obtain a homogeneous glass by tuning the O/P ratio or the AgI content. The presence of AgI residues seems to indicate that there is an excess of such phase and that its amount must be reduced in order to obtain a single-phase glass matrix. AgI is formed because of the reaction between Ag^0 (formed during the pyrolysis step) and gaseous iodine. Therefore, to reduce the AgI content, it is necessary to reduce the initial quantity of Ag^0 into the sorbent. For that, silver reduction rate during pyrolysis should be controlled. This could be done by several means: adjusting the dwell duration and/or its temperature [63]–[65],

317 modulating the alginate/Ag_3PO_4 ratio [65] or the O_2 partial pressure [66]. These different
318 parameters offer many perspectives to this work in order to obtain a homogeneous matrix.
319 Concerning calcium which is completely excluded from the glass network by formation of
320 $Ca_2P_2O_7$ crystals, no data is referenced regarding a potential incorporation of this phase into an
321 iodine silver phosphate glass.

322 ## *5* Conclusion

323 A new route for the synthesis of silver phosphate-based iodine filters has been
324 developed. These filters intend to be used as precursors to obtain an iodine-containing
325 conditioning matrix by direct vitrification. Sodium alginate was used to modulate the shape of
326 these filters by forming beads. These beads kept their initial form after pyrolysis at 500 °C to
327 remove organic material. Upon pyrolysis, a reduction of cationic silver into Ag^0 also occurred
328 and it was ascribed to reducing properties of alginate molecules. Iodine capture of the obtained
329 sorbent in static conditions at 110 °C showed a capture rate of 470 $mg.g^{-1}$ in spite of a low
330 specific surface area. During the vitrification of the iodine-loaded sorbent at 650 °C, very few
331 quantities of iodine were lost (< 0.2 $\%_{wt}$) and a glass incorporating iodine was obtained. The
332 final material was multiphasic and contained glass phase, Ag^0, AgI and $Ca_2P_2O_7$.
333 This work hints at the possibility of a direct transformation of iodine-loaded filters into a
334 conditioning matrix by thermal treatment with a low iodine volatilization. In the context of the
335 storage of radioactive iodine in a deep geological repository, this type of one-step process could
336 be very advantageous. In order to optimize the final microstructure and get a homogeneous
337 glass with no trace of excess AgI, it is of importance to tune the progress of reduction upon the
338 pyrolysis step.

339 ## Acknowledgements

340 We thank PRIME Verre (France) for assistance with BET(Kr) measurements.

6 References

[1] J. Bongaarts, "Human population growth and the demographic transition," *Philos. Trans. R. Soc. B Biol. Sci.*, vol. 364, no. 1532, pp. 2985–2990, Oct. 2009, doi: 10.1098/rstb.2009.0137.

[2] J. Cleland, "World Population Growth; Past, Present and Future," *Environ. Resour. Econ.*, vol. 55, no. 4, pp. 543–554, Aug. 2013, doi: 10.1007/s10640-013-9675-6.

[3] J. P. DeLong and O. Burger, "Socio-Economic Instability and the Scaling of Energy Use with Population Size," *PLOS ONE*, vol. 10, no. 6, p. e0130547, Jun. 2015, doi: 10.1371/journal.pone.0130547.

[4] M. Tashimo and K. Matsui, "Role of nuclear energy in environment, economy, and energy issues of the 21st century – Growing energy demand in Asia and role of nuclear," *Prog. Nucl. Energy*, vol. 50, no. 2, pp. 103–108, Mar. 2008, doi: 10.1016/j.pnucene.2007.10.024.

[5] R. J. Baker, "Uranium minerals and their relevance to long term storage of nuclear fuels," *Coord. Chem. Rev.*, vol. 266–267, pp. 123–136, May 2014, doi: 10.1016/j.ccr.2013.10.004.

[6] J. Kim, H. Yoon, D. Kook, and Y. Kim, "A STUDY ON THE INITIAL CHARACTERISTICS OF DOMESTIC SPENT NUCLEAR FUELS FOR LONG TERM DRY STORAGE," *Nucl. Eng. Technol.*, vol. 45, no. 3, pp. 377–384, Jun. 2013, doi: 10.5516/NET.06.2012.082.

[7] D. Olander, "Nuclear fuels – Present and future," *J. Nucl. Mater.*, vol. 389, no. 1, pp. 1–22, May 2009, doi: 10.1016/j.jnucmat.2009.01.297.

[8] R. Natarajan, "Reprocessing of spent nuclear fuel in India: Present challenges and future programme," *Prog. Nucl. Energy*, vol. 101, pp. 118–132, Nov. 2017, doi: 10.1016/j.pnucene.2017.03.001.

[9] C. Ory *et al.*, "Consequences of atmospheric contamination by radioiodine: the Chernobyl and Fukushima accidents," *Endocrine*, vol. 71, no. 2, pp. 298–309, Feb. 2021, doi: 10.1007/s12020-020-02498-9.

[10] S. Yamashita, S. Suzuki, S. Suzuki, H. Shimura, and V. Saenko, "Lessons from Fukushima: Latest Findings of Thyroid Cancer After the Fukushima Nuclear Power Plant Accident," *Thyroid*, vol. 28, no. 1, pp. 11–22, Sep. 2017, doi: 10.1089/thy.2017.0283.

[11] J. Robbins and A. B. Schneider, "Thyroid Cancer Following Exposure to Radioactive Iodine," *Rev. Endocr. Metab. Disord.*, vol. 1, no. 3, pp. 197–203, Apr. 2000, doi: 10.1023/A:1010031115233.

[12] H. Koch-Steindl and G. Pröhl, "Considerations on the behaviour of long-lived radionuclides in the soil," *Radiat. Environ. Biophys.*, vol. 40, no. 2, pp. 93–104, Jun. 2001, doi: 10.1007/s004110100098.

[13] F. Köhler, B. Riebe, A. Weller, and C. Walther, "Determination of iodine mobility in the soil vadose zone using long-term column experiments," *J. Radioanal. Nucl. Chem.*, vol. 322, no. 3, pp. 1755–1760, Dec. 2019, doi: 10.1007/s10967-019-06789-y.

[14] S. Zhang *et al.*, "Concentration-Dependent Mobility, Retardation, and Speciation of Iodine in Surface Sediment from the Savannah River Site," *Environ. Sci. Technol.*, vol. 45, no. 13, pp. 5543–5549, Jul. 2011, doi: 10.1021/es1040442.

[15] V. Alfimov, A. Aldahan, G. Possnert, A. Kekli, and M. Meili, "Concentrations of 129I along a transect from the North Atlantic to the Baltic Sea," *Nucl. Instrum. Methods Phys. Res. Sect. B Beam Interact. Mater. At.*, vol. 223–224, pp. 446–450, Aug. 2004, doi: 10.1016/j.nimb.2004.04.084.

[16] C. Fréchou and D. Calmet, "129I in the environment of the La Hague nuclear fuel reprocessing plant—from sea to land," *J. Environ. Radioact.*, vol. 70, no. 1, pp. 43–59, Jan. 2003, doi: 10.1016/S0265-931X(03)00127-9.
[17] W. Xie, D. Cui, S.-R. Zhang, Y.-H. Xu, and D.-L. Jiang, "Iodine capture in porous organic polymers and metal–organic frameworks materials," *Mater. Horiz.*, vol. 6, no. 8, pp. 1571–1595, Sep. 2019, doi: 10.1039/C8MH01656A.
[18] D. F. Sava, T. J. Garino, and T. M. Nenoff, "Iodine Confinement into Metal–Organic Frameworks (MOFs): Low-Temperature Sintering Glasses To Form Novel Glass Composite Material (GCM) Alternative Waste Forms," *Ind. Eng. Chem. Res.*, vol. 51, no. 2, pp. 614–620, Jan. 2012, doi: 10.1021/ie200248g.
[19] A. I. Wiechert *et al.*, "Capture of Iodine from Nuclear-Fuel-Reprocessing Off-Gas: Influence of Aging on a Reduced Silver Mordenite Adsorbent after Exposure to NO/NO2," *ACS Appl. Mater. Interfaces*, vol. 12, no. 44, pp. 49680–49693, Nov. 2020, doi: 10.1021/acsami.0c15456.
[20] Y. Nan, L. L. Tavlarides, and D. W. DePaoli, "Adsorption of iodine on hydrogen-reduced silver-exchanged mordenite: Experiments and modeling," *AIChE J.*, Aug. 2016, doi: 10.1002/aic.15432.
[21] B. Azambre and M. Chebbi, "Evaluation of Silver Zeolites Sorbents Toward Their Ability to Promote Stable CH3I Storage as AgI Precipitates," *ACS Appl. Mater. Interfaces*, vol. 9, no. 30, pp. 25194–25203, Aug. 2017, doi: 10.1021/acsami.7b02366.
[22] K. S. Subrahmanyam *et al.*, "Chalcogenide Aerogels as Sorbents for Radioactive Iodine," *Chem. Mater.*, vol. 27, no. 7, pp. 2619–2626, Apr. 2015, doi: 10.1021/acs.chemmater.5b00413.
[23] B. J. Riley *et al.*, "Chalcogen-based aerogels as a multifunctional platform for remediation of radioactive iodine," *RSC Adv.*, vol. 1, no. 9, pp. 1704–1715, Nov. 2011, doi: 10.1039/C1RA00351H.
[24] B. J. Riley, S. Chong, M. J. Olszta, and J. A. Peterson, "Evaluation of Getter Metals in Na–Al–Si–O Aerogels and Xerogels for the Capture of Iodine Gas," *ACS Appl. Mater. Interfaces*, vol. 12, no. 17, pp. 19682–19692, Apr. 2020, doi: 10.1021/acsami.0c03155.
[25] J. Matyáš, G. E. Fryxell, B. J. Busche, K. Wallace, and L. S. Fifield, "Functionalized Silica Aerogels: Advanced Materials to Capture and Immobilize Radioactive Iodine," in *Ceramic Materials for Energy Applications*, John Wiley & Sons, Ltd, 2011, pp. 21–32. doi: 10.1002/9781118095386.ch3.
[26] S. Chong, B. J. Riley, J. A. Peterson, M. J. Olszta, and Z. J. Nelson, "Gaseous Iodine Sorbents: A Comparison between Ag-Loaded Aerogel and Xerogel Scaffolds," *ACS Appl. Mater. Interfaces*, vol. 12, no. 23, pp. 26127–26136, Jun. 2020, doi: 10.1021/acsami.0c02396.
[27] K. Ho, D. Park, M.-K. Park, and C.-H. Lee, "Adsorption mechanism of methyl iodide by triethylenediamine and quinuclidine-impregnated activated carbons at extremely low pressures," *Chem. Eng. J.*, vol. 396, p. 125215, Sep. 2020, doi: 10.1016/j.cej.2020.125215.
[28] H. Sun, B. Yang, and A. Li, "Biomass derived porous carbon for efficient capture of carbon dioxide, organic contaminants and volatile iodine with exceptionally high uptake," *Chem. Eng. J.*, vol. 372, pp. 65–73, Sep. 2019, doi: 10.1016/j.cej.2019.04.061.
[29] K. Ho, S. Moon, H. C. Lee, Y. K. Hwang, and C.-H. Lee, "Adsorptive removal of gaseous methyl iodide by triethylenediamine (TEDA)-metal impregnated activated carbons under humid conditions," *J. Hazard. Mater.*, vol. 368, pp. 550–559, Apr. 2019, doi: 10.1016/j.jhazmat.2019.01.078.
[30] B. Liu *et al.*, "High efficient adsorption and storage of iodine on S, N co-doped graphene aerogel," *J. Hazard. Mater.*, vol. 373, pp. 705–715, Jul. 2019, doi: 10.1016/j.jhazmat.2019.04.005.

[31] S. Han, W. Um, and W.-S. Kim, "Development of bismuth-functionalized graphene oxide to remove radioactive iodine," *Dalton Trans.*, vol. 48, no. 2, pp. 478–485, 2019, doi: 10.1039/C8DT03745K.
[32] S. M. Scott, T. Hu, T. Yao, G. Xin, and J. Lian, "Graphene-based sorbents for iodine-129 capture and sequestration," *Carbon*, vol. 90, pp. 1–8, Aug. 2015, doi: 10.1016/j.carbon.2015.03.070.
[33] S. A. Kulyukhin, L. V. Mizina, E. V. Zanina, I. A. Rumer, N. A. Konovalova, and D. S. Levushkin, "Synthesis of sorbents based on coarsely dispersed silica gel, containing nanoparticles of Ag compounds, for localization of volatile radioactive iodine compounds from the water vapor-air medium," *Radiochemistry*, vol. 54, no. 4, pp. 368–378, Jul. 2012, doi: 10.1134/S1066362212040108.
[34] Daryl Haefner, "Methods of Gas Phase Capture of Iodine from Fuel Reprocessing Off-Gas: A Literature Survey," INL/EXT-07-12299, 911962, Feb. 2007. doi: 10.2172/911962.
[35] T. Fukasawa, "Influences of Impurities on Iodine Removal Efficiency of Silver Alumina Adsorbent," Proceedings of the 24th DOE/NRC Nuclear Air Cleaning and Treatment Conference, United-States, NUREG/CP-0153; CONF-960715-, Aug. 1997.
[36] J. Huve, A. Ryzhikov, H. Nouali, V. Lalia, G. Augé, and T. J. Daou, "Porous sorbents for the capture of radioactive iodine compounds: a review," *RSC Adv.*, vol. 8, no. 51, pp. 29248–29273, Aug. 2018, doi: 10.1039/C8RA04775H.
[37] S. U. Nandanwar, K. Coldsnow, V. Utgikar, P. Sabharwall, and D. Eric Aston, "Capture of harmful radioactive contaminants from off-gas stream using porous solid sorbents for clean environment – A review," *Chem. Eng. J.*, vol. 306, pp. 369–381, Dec. 2016, doi: 10.1016/j.cej.2016.07.073.
[38] B. J. Riley, J. D. Vienna, D. M. Strachan, J. S. McCloy, and J. L. Jerden, "Materials and processes for the effective capture and immobilization of radioiodine: A review," *J. Nucl. Mater.*, vol. 470, pp. 307–326, Mar. 2016, doi: 10.1016/j.jnucmat.2015.11.038.
[39] J. H. Yang, H.-S. Park, and Y.-Z. Cho, "Al2O3-containing silver phosphate glasses as hosting matrices for radioactive iodine," *J. Nucl. Sci. Technol.*, vol. 54, no. 12, pp. 1330–1337, Dec. 2017, doi: 10.1080/00223131.2017.1365025.
[40] M. ul Hassan, S. Venkatesan, and H. J. Ryu, "Non-volatile immobilization of iodine by the cold-sintering of iodosodalite," *J. Hazard. Mater.*, vol. 386, p. 121646, Mar. 2020, doi: 10.1016/j.jhazmat.2019.121646.
[41] A. Coulon, D. Laurencin, A. Grandjean, C. C. D. Coumes, S. Rossignol, and L. Campayo, "Immobilization of iodine into a hydroxyapatite structure prepared by cementation," *J. Mater. Chem. A*, vol. 2, no. 48, pp. 20923–20932, Nov. 2014, doi: 10.1039/C4TA03236E.
[42] J. H. Yang, H.-S. Park, and Y.-Z. Cho, "Silver phosphate glasses for immobilization of radioactive iodine," *Ann. Nucl. Energy*, vol. 110, pp. 208–214, Dec. 2017, doi: 10.1016/j.anucene.2017.06.042.
[43] A.-L. Chabauty, F. O. Méar, L. Montagne, and L. Campayo, "Chemical durability evaluation of silver phosphate–based glasses designed for the conditioning of radioactive iodine," *J. Nucl. Mater.*, vol. 550, p. 152919, Jul. 2021, doi: 10.1016/j.jnucmat.2021.152919.
[44] A.-L. Chabauty, L. Campayo, F. O. Méar, and L. Montagne, "Niobium- and bismuth-silver phosphate glasses for the conditioning of radioactive iodine," *J. Non-Cryst. Solids*, vol. 510, pp. 51–61, Apr. 2019, doi: 10.1016/j.jnoncrysol.2019.01.015.
[45] T. Minami, Y. Takuma, and M. Tanaka, "Superionic Conducting Glasses: Glass Formation and Conductivity in the AgI - Ag2 O - P 2 O 5 System," *J. Electrochem. Soc.*, vol. 124, no. 11, p. 1659, Nov. 1977, doi: 10.1149/1.2133131.
[46] H. Fujihara, T. Murase, T. Nishi, K. Noshita, T. Yoshida, and M. Matsuda, "Low temperature vitrification of radioiodine using AgI-Ag_2O-P_2O_5 glass system," *Sci. Basis*

Nucl. Waste Manag. XXII Mater. Res. Soc. Symp. Proc. Vol. 556, 1999, Accessed: Apr. 09, 2021. [Online]. Available: http://inis.iaea.org/Search/search.aspx?orig_q=RN:31020786

[47] M. Chee Kimling, N. Scales, T. L. Hanley, and R. A. Caruso, "Uranyl-Sorption Properties of Amorphous and Crystalline TiO2/ZrO2 Millimeter-Sized Hierarchically Porous Beads," *Environ. Sci. Technol.*, vol. 46, no. 14, pp. 7913–7920, Jul. 2012, doi: 10.1021/es3011157.

[48] M. C. Kimling and R. A. Caruso, "Sol–gel synthesis of hierarchically porous TiO2 beads using calcium alginate beads as sacrificial templates," *J. Mater. Chem.*, vol. 22, no. 9, pp. 4073–4082, Feb. 2012, doi: 10.1039/C2JM15720A.

[49] G. Ionita, A. M. Ariciu, D. K. Smith, and V. Chechik, "Ion exchange in alginate gels – dynamic behaviour revealed by electron paramagnetic resonance," *Soft Matter*, vol. 11, no. 46, pp. 8968–8974, Nov. 2015, doi: 10.1039/C5SM02062J.

[50] K. Y. Lee and D. J. Mooney, "Alginate: Properties and biomedical applications," *Prog. Polym. Sci.*, vol. 37, no. 1, pp. 106–126, Jan. 2012, doi: 10.1016/j.progpolymsci.2011.06.003.

[51] F. Abasalizadeh *et al.*, "Alginate-based hydrogels as drug delivery vehicles in cancer treatment and their applications in wound dressing and 3D bioprinting," *J. Biol. Eng.*, vol. 14, p. 8, 2020, doi: 10.1186/s13036-020-0227-7.

[52] R. D. Scheele, L. L. Burger, and C. L. Matsuzaki, "Methyl Iodide Sorption by Reduced Silver Mordenite," Jun. 1983. doi: 10.2172/6017408.

[53] P. S. Kumar, P. B. Dayal, and C. S. Sunandana, "On the formation mechanism of γ-AgI thin films," *Thin Solid Films*, vol. 357, no. 2, pp. 111–118, Dec. 1999, doi: 10.1016/S0040-6090(99)00647-1.

[54] K. W. Chapman, P. J. Chupas, and T. M. Nenoff, "Radioactive Iodine Capture in Silver-Containing Mordenites through Nanoscale Silver Iodide Formation," *J. Am. Chem. Soc.*, vol. 132, no. 26, pp. 8897–8899, Jul. 2010, doi: 10.1021/ja103110y.

[55] I. X. Yin, J. Zhang, I. S. Zhao, M. L. Mei, Q. Li, and C. H. Chu, "The Antibacterial Mechanism of Silver Nanoparticles and Its Application in Dentistry," *Int. J. Nanomedicine*, vol. 15, pp. 2555–2562, Apr. 2020, doi: 10.2147/IJN.S246764.

[56] B. Le Ouay and F. Stellacci, "Antibacterial activity of silver nanoparticles: A surface science insight," *Nano Today*, vol. 10, no. 3, pp. 339–354, Jun. 2015, doi: 10.1016/j.nantod.2015.04.002.

[57] J. Yang and J. Pan, "Hydrothermal synthesis of silver nanoparticles by sodium alginate and their applications in surface-enhanced Raman scattering and catalysis," *Acta Mater.*, vol. 60, no. 12, pp. 4753–4758, Jul. 2012, doi: 10.1016/j.actamat.2012.05.037.

[58] X. Zhao *et al.*, "Microwave-assisted synthesis of silver nanoparticles using sodium alginate and their antibacterial activity," *Colloids Surf. Physicochem. Eng. Asp.*, vol. 444, pp. 180–188, Mar. 2014, doi: 10.1016/j.colsurfa.2013.12.008.

[59] A. Pal, K. Esumi, and T. Pal, "Preparation of nanosized gold particles in a biopolymer using UV photoactivation," *J. Colloid Interface Sci.*, vol. 288, no. 2, pp. 396–401, Aug. 2005, doi: 10.1016/j.jcis.2005.03.048.

[60] T. Takahashi, S. Ikeda, and O. Yamamoto, "Solid-State Ionics—Solids with High Ionic Conductivity in the Systems Silver Iodide-Silver Oxyacid Salts," *J. Electrochem. Soc.*, vol. 119, no. 4, p. 477, Apr. 1972, doi: 10.1149/1.2404235.

[61] A. Doi, H. Hayakawa, and H. Kamioka, "Ultrasonic study of (AgI)x(Ag4P2O7)1-x glasses in the region of the glass-transition temperature," *Phys. Rev. B*, vol. 47, no. 21, pp. 14136–14141, Jun. 1993, doi: 10.1103/PhysRevB.47.14136.

[62] "Ultrasonic study of liquid-quenched (AgI)x(Ag3PO4)1−x compared with (AgI)x(Ag4P2O7)1−x", doi: 10.1007/bf00355866.

[63] X. Jiang, W. Chen, C. Chen, S. Xiong, and A. Yu, "Role of Temperature in the Growth of Silver Nanoparticles Through a Synergetic Reduction Approach," *Nanoscale Res. Lett.*, vol. 6, no. 1, p. 32, Sep. 2010, doi: 10.1007/s11671-010-9780-1.

[64] N. Fleitas-Salazar, E. Silva-Campa, S. Pedroso-Santana, J. Tanori, M. R. Pedroza-Montero, and R. Riera, "Effect of temperature on the synthesis of silver nanoparticles with polyethylene glycol: new insights into the reduction mechanism," *J. Nanoparticle Res.*, vol. 19, no. 3, p. 113, Mar. 2017, doi: 10.1007/s11051-017-3780-3.

[65] I. Pastoriza-Santos and L. M. Liz-Marzán, "Reduction of silver nanoparticles in DMF. Formation of monolayers and stable colloids," *Pure Appl. Chem.*, vol. 72, no. 1–2, pp. 83–90, Jan. 2000, doi: 10.1351/pac200072010083.

[66] M.-H. Chopinet, D. Lizarazu, and C. Rocanière, "L'importance des phénomènes d'oxydo-réduction dans le verre," *Comptes Rendus Chim.*, vol. 5, no. 12, pp. 939–949, Dec. 2002, doi: 10.1016/S1631-0748(02)01455-8.